

Presented at the 29th Kraków School of Theoretical Physics,  
Zakopane, June 1999 (Acta Physica Polonica B – 1999/2000).

## DIAGNOSIS OF QGP WITH STRANGE HADRONS

JAN RAFELSKI<sup>†</sup>

Department of Physics, University of Arizona, Tucson, AZ 85721

AND

JEAN LETESSIER

Laboratoire de Physique Théorique et Hautes Energies<sup>‡</sup>  
Université Paris 7, 2 place Jussieu, F-75251 Cedex 05

We review the current status of strangeness as signature of the formation and dissociation of the deconfined QGP at the SPS energy scale, and present the status of our considerations for RHIC energies. By analyzing, within the framework of a Fermi statistical model, the hadron abundance and spectra, the properties of a disintegrating, hadron evaporating, deconfined QGP fireball are determined and can be compared with theory for the energy range 160–200 A GeV on fixed target. We discuss in more detail our finding that the pion yields occur near to pion condensation condition. Dynamical models of chemical strangeness equilibration are developed and applied to obtain strangeness production in a QGP phase at conditions found at SPS and expected at RHIC. The sudden QGP break up model that works for the SPS data implies at RHIC dominance of both baryon, and antibaryon, abundances by the strange baryon and antibaryon yields.

PACS numbers: 12.38.Mh, 25.75.-q, 25.75.Dw, 25.75.Ld

### 1. Introduction

Strange particle signatures for the formation and evolution of the deconfined quark-gluon phase of elementary matter (QGP) has been a subject developed quite intensely for the past 20 years. We review here our progress since the last major review [1], highlighting our analysis of the Pb–Pb data at SPS, and our predictions for hyperon yields from QGP at RHIC [2].

We first describe in section 2, the Fermi model [3] analysis of the multi-particle production processes in 158 A GeV Pb–Pb collisions carried out at

---

<sup>†</sup> Support by U.S. Department of Energy under grant DE-FG03-95ER40937.

<sup>‡</sup> LPTHE, Univ. Paris 6 et 7 is: Unité mixte de Recherche du CNRS, UMR7589.

CERN-SPS. Strongly interacting particles are believed to be produced with a probability commensurating to the size of the accessible phase space. The numerical methods which have been developed in the context of an analysis of the lighter 200A GeV S–Au/W/Pb system [4] are described. We have in particular shown [5, 6] that consideration of the light quark chemical non-equilibrium is necessary in order to arrive at a consistent interpretation of the experimental results of both the wide acceptance NA49-experiment [7, 8, 9, 10, 11] and central rapidity strange (multi)strange (anti)baryon WA97-experiment [12, 13, 14]. This resulted also in considerable reduction of the chemical freeze-out temperature: we find  $T_f = 145 \pm 5$  MeV, while originally it has been estimated to be [15, 16]  $T_f = 180\text{--}290$  MeV.

Such a low freeze-out temperature is more consistent with the assumption we make that there is no change of hadronic particle abundance after the deconfined QGP source has dissociated. This scheme is called *sudden hadronization* [17, 18]. This can occur if hadronic particles are produced either in:

- a) an evaporation process from a hot expanding, surface or
- b) a sudden global hadronization process.

Our sudden hadronization scheme works very well, and can be considered as established on view of many studies that could describe quite diverse data. Certain surprising features of Pb–Pb results that are seen within such analysis, and in particular the finding that the pion yield is governed by a fugacity that is close to the condensation point, as we shall show in section 3, lead us presently to favor the scenario b). That being the case one may further suppose that a super-cooled plasma occupies a relatively large spatial volume, and it undergoes a global explosive decomposition into individual hadrons, maximizing hadron occupancies and thus the entropy content in the confined phase at the near-pion-condensation condition.

Pertinent results of our analysis of the Pb–Pb system are addressed in section 3, where we have reevaluated our current results in consideration of some small change of the experimental data. We address all available SPS NA49 and WA97 experimental data, except for  $\Omega$  and  $\bar{\Omega}$  particles. It is important to realize that if we succeed to describe well a particle yield within the Fermi model, it means that the majority of all particles of the particular type is produced by the statistical mechanisms we address here. In principle there could be many other production mechanisms, and they add to the yields. Thus if our description fail, an acceptable failure is the one which *under-predicts the yield*. When statistical model predicts very little if any production, the other reaction pictures may indeed be dominant and we should at least hesitate in our attempt to describe all the rare particle yields. The prime candidate for such consideration and omission from statistical analysis is the totally strange  $\Omega(sss)$  and its antiparticle: they are

triply strangeness suppressed and are very heavy with  $M_\Omega = 1672$  MeV, thus again significantly suppressed, especially at low chemical freeze-out temperature. Their total statistical multiplicity is by a good distance smallest of all ‘stable’ hadrons. Consequently, their production pattern is easily altered by, *e.g.*, in source strangeness clustering. We have found that if we use the results we obtain about the properties of the source [6], in order to compute the yields of  $\Omega$  and  $\bar{\Omega}$ , we invariably see that we obtain only a fraction, 40–50%, of all particles observed. Our preliminary conclusion is that we should NOT explore these particles in the statistical production model.

Among results that we obtain in section 3 is the, on a first sight, surprising overpopulation of the strangeness phase space occupancy. We explain how this can occur in section 4, where the kinetic theory for computation of the chemical strangeness flavor abundance equilibration is presented. We extend our past study of strangeness production at SPS conditions and show that, at the time of QGP breakup at RHIC energies, there is also in general full chemical equilibrium, indeed that one can expect over-saturation of strangeness flavor, just as at SPS. Our numerical study is based on the dynamics of the phase space occupancy rather than particle density, and we eliminate much of the dependence on the dynamical flow effects by incorporating in the dynamics considered the hypothesis of entropy conserving matter flow and evolution. We will make two assumptions of relevance for the results we obtain:

- the kinetic (momentum distribution) equilibrium is reached faster than the chemical (abundance) equilibrium [19, 20];
- gluons equilibrate chemically significantly faster than strangeness [21].

The first assumption allows to study only the chemical abundances, rather than the full momentum distribution, which simplifies greatly the structure of the master equations; the second assumption allows to focus after an initial time  $\tau_0$  has passed on the evolution of strangeness population:  $\tau_0$  is the time required for the development to near chemical equilibrium of the gluon population. As we shall see, the strange quark mass  $m_s$  is the only undetermined parameter that enters strangeness yield calculations. The overpopulation of the strangeness phase space, seen in SPS data arises for relatively small  $m_s(1\text{GeV}) \simeq 200$  MeV.

In the following section 5, we use the experience we have with the SPS systems and with the theoretical studies of strangeness production in QGP, in order to estimate the strange particle production that is likely to occur at RHIC. Some remarkable particle abundance results arise, since during the break-up of the QGP phase there is considerable advantage for strangeness flavor to stick to baryons. This can be easily understood considering that production of strange baryons over kaons is favored by the energy balance, *i.e.* :  $E(\Lambda + \pi) < E(N+K)$ . Since at RHIC most hadrons produced are

mesons, and baryons form just a small fraction of all particles, initially we expect and will show, in section 5, that hyperon production dominates baryon production, *i.e.*, most baryons and antibaryons produced will be strange. A remarkable consequence of the sudden hadronization scenario is that this situation is maintained and thus hyperon dominance should be observed at RHIC. If indeed this prediction is born out in the experiment, it will prove that there was formation of deconfined phase, followed by sudden hadronization.

We note that at SPS energies described in section 3, there is still an appreciable relative baryon abundance among all hadrons (about 15%) and thus while hyperon dominance begins to set in, there are (literally speaking) still some non-strange baryons left. With increasing energy the yield of strange quark pairs per baryon rises, and at the same time the relative abundance of baryons among all hadrons diminishes, the relative population of non-strange baryons decreases rather rapidly and at RHIC energies the hyperons and/or antihyperons are the dominant strange particle fractions.

We are not aware that other studies reported in literature about RHIC conditions have this remarkable result, see, *e.g.*, [22]. It is thus interesting to record the two major quantitative differences of the behavior of deconfined matter we are considering:

- in QGP the particle density is high enough to assure that the required abundance of strangeness can be actually produced [1, 23, 24, 25], while in hadron phase it was shown that, even at SPS energy, this is not the case [26].
- overpopulation of hadron phase space occupancies occurs naturally when the entropy rich QGP phase disintegrates into hadrons, which cannot be expected in hadron based kinetic reactions.

## 2. Contemporary Fermi model of Hadron Production

We use 6 parameters to characterize the spectra and abundances of particles. Will describe these discussing their values, assuming a QGP source:

- 1) The strange quark fugacity  $\lambda_s = 1$  can be obtained from the requirement that strangeness balances [27]:

$$\langle N_s - N_{\bar{s}} \rangle = 0. \quad (1)$$

However, the Coulomb distortion of the strange quark phase space plays an important role in the understanding of this constraint for Pb–Pb collisions [5], leading to the Coulomb-deformed value  $\lambda_s = 1.10$ , see also Eq. (10).

- 2) Strange quark phase space occupancy  $\gamma_s$  can be computed as we show in section 4 within the established kinetic theory framework for strangeness production [1, 23]. For a rapidly expanding system the production processes will lead to an oversaturated phase space with  $\gamma_s > 1$ .

3) The equilibrium phase space occupancy of light quarks  $\gamma_q$  is expected to exceed unity significantly to accommodate the excess entropy content in the plasma phase [27]. There is an interesting constraint that arises if hadronization is sudden in the sense that particles are produced at the same time, forming for pions a Bose gas. As we shall discuss at the end of this section, see Eq. (9) this leads to an upper limit:

$$\gamma_q < \gamma_q^c \equiv e^{m_\pi/2T}. \quad (2)$$

4) The collective surface expansion velocity should remain below the relativistic sound velocity [1]:

$$v_c \leq 1/\sqrt{3}. \quad (3)$$

5,6) If we assume that the stopping of the baryon number and energy is similar [1], we know the energy per baryon content in the reactions and then the equations of state produce a further constraint between chemical freeze-out temperature  $T_f$  and light quark fugacity  $\lambda_q$  or equivalently, the baryochemical potential:

$$\mu_B = 3 T_f \ln \lambda_q. \quad (4)$$

The difference between  $\lambda_i$  and  $\gamma_i$  is that, *e.g.*, for strange and anti-strange quarks the same factor  $\gamma_s$  applies, while the antiparticle fugacity is inverse of the particle fugacity. The proper statistical physics foundation of  $\gamma_i$  is obtained considering the maximum entropy principle: it has been determined that while the limit  $\gamma_i \rightarrow 1$  maximizes the specific chemical entropy, this maximum is extremely shallow, indicating that a system with dynamically evolving volume will in general find more effective paths to increase entropy, than offered by the establishment of the absolute chemical equilibrium [28].

The abundances of the final state particles is most conveniently described by considering the phase space distribution of particles. The relative number of primary particles freezing out from a source is obtained noting that the fugacity and phase space occupancy of a composite hadronic particle is expressed by its constituents and that the probability to find all  $j$ -components contained within the  $i$ -th emitted particle is:

$$N_i \propto e^{-E_i/T} \prod_{j \in i} \gamma_j \lambda_j, \quad \lambda_i = \prod_{j \in i} \lambda_j, \quad \gamma_i = \prod_{j \in i} \gamma_j. \quad (5)$$

Taking the Laplace transform, we find, *e.g.*, for the strange sector, to the following partition function, like expression:

$$\ln \mathcal{Z}_s = \frac{VT^3}{2\pi^2} \left\{ (\lambda_s \lambda_q^{-1} + \lambda_s^{-1} \lambda_q) \gamma_s \gamma_q C_M^s F_K + (\lambda_s \lambda_q^2 + \lambda_s^{-1} \lambda_q^{-2}) \gamma_s \gamma_q^2 C_B^s F_Y \right. \\ \left. + (\lambda_s^2 \lambda_q + \lambda_s^{-2} \lambda_q^{-1}) \gamma_s^2 \gamma_q C_B^s F_\Xi + (\lambda_s^3 + \lambda_s^{-3}) \gamma_s^3 C_B^s F_\Omega \right\}, \quad (6)$$

where the kaon, hyperon, cascade and omega degrees of freedom are included. The phase space factors  $F_i$  of the strange particles are (with  $g_i$  describing the statistical degeneracy):

$$F_i = \sum_j g_{ij} W(m_{ij}/T) . \quad (7)$$

In the resonance sums  $\sum_j$  all known strange hadrons should be counted. The function  $W(x) = x^2 K_2(x)$ , where  $K_2$  is the modified Bessel function, arises from the phase-space integral of the different particle distributions  $f(\vec{p})$ . It is important to remember that this expression does not describe the properties of a gas of hadrons, thus it is not a partition function, even if we give the Laplace transform of the phase space such formal semblance.

When the source of the particles is subject to flow, the Laplace transform that leads to the above expression is considerably more involved. the spectra and thus also multiplicities of particles emitted are obtained replacing the Boltzmann factor in Eq. (5) by [29]:

$$e^{-E_i/T} \rightarrow \frac{1}{2\pi} \int d\Omega_v \gamma_c (1 - \vec{v}_c \cdot \vec{p}_i/E_i) e^{-\frac{\gamma_c E_i}{T} (1 - \vec{v}_c \cdot \vec{p}_i/E_i)},$$

$$\gamma_c = \frac{1}{\sqrt{1 - \vec{v}_c^2}}, \quad (8)$$

a result which can be intuitively obtained by a Lorentz transformation between an observer on the surface of the fireball, and one at rest in laboratory frame. In certain details the results we obtain confirm the applicability of this simple approach. We consider for SPS energy range the radial flow model, perhaps the simplest of the complex flow cases possible, but it suffices to fully assess the impact of flow on our analysis.

While the integral over the entire phase space of the flow spectrum yields as many particles with and without flow, when acceptance cuts are present particles of different mass experience differing flow effects. Here, we note that the final particle abundances measured in an experiment are obtained after all unstable hadronic resonances are allowed to disintegrate and feed the stable hadron spectra. In order to minimize the impact of unknown flow pattern at hadron freeze-out when considering particle abundances measured in a restricted phase space domain, we study particle abundance ratios involving what we call compatible hadrons: these are particles likely to be impacted in a similar fashion by collective flow dynamics in the fireball.

We now return to review the case of pions, which is exceptional since we will be considering a rather large values of  $\gamma_q > 1.5$ . The chemical fugacity for a particle composed of a light quark-antiquark pair is  $\gamma_q^2$ . Thus the Bose

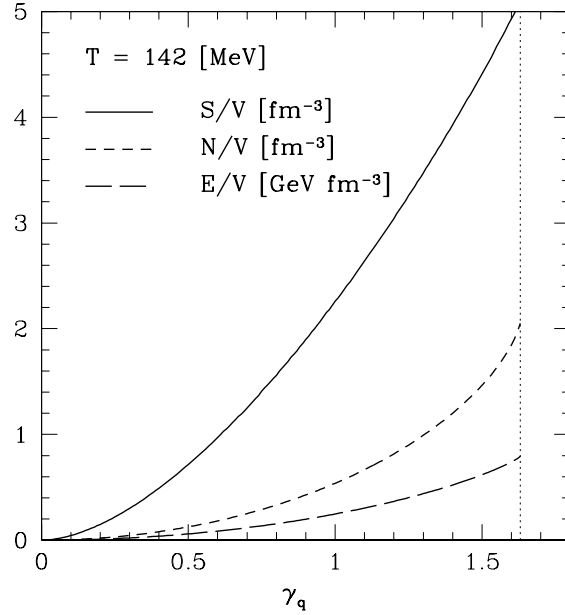


Fig. 1. Dependence of pion gas properties  $N/V$ -particle,  $E/V$ -energy and  $S/V$ -entropy density, as function of  $\gamma_q$  at  $T = 142$  MeV.

distribution in momentum space has the shape:

$$f_\pi(E) = \frac{1}{\gamma_q^{-2} e^{E_\pi/T} - 1}, \quad E_\pi = \sqrt{m_\pi^2 + p^2}. \quad (9)$$

The range of values for  $\gamma_q$  is bounded from above by the Bose singularity. When  $\gamma_q \rightarrow \gamma_q^c$ , see Eq. (2), the lowest energy state (in the continuum limit with  $p \rightarrow 0$ ) will acquire macroscopic occupation and a pion condensate is formed. Such a condensate ‘consumes’ energy without consuming entropy of the primordial high entropy QGP phase. Thus a condensate is not likely to develop, but the hadronization process may have the tendency to approach the limiting value in order to more efficiently connect the deconfined and the confined phases, since, as we show in Fig. 1, the entropy density is nearly twice as high at  $\gamma_q \simeq \gamma_q^c$  than at  $\gamma_q = 1$ .

To see clearly how this can occur, we looked more closely at the relative properties of a pion gas for  $\gamma_q \rightarrow \gamma_q^c$ . In Fig. 2, we see the relative change in energy per pion, (inverse of) entropy per pion, and energy per entropy, for fixed  $T = 142$  MeV corresponding to our best fit condition. We see that a hadronizing gas will consume at higher  $\gamma_q$  less energy per particle, and that the energy per entropy is nearly constant. Dissociation into pions at  $\gamma_q \rightarrow \gamma_q^c$  appears thus to be an effective way to convert excess of entropy in the plasma

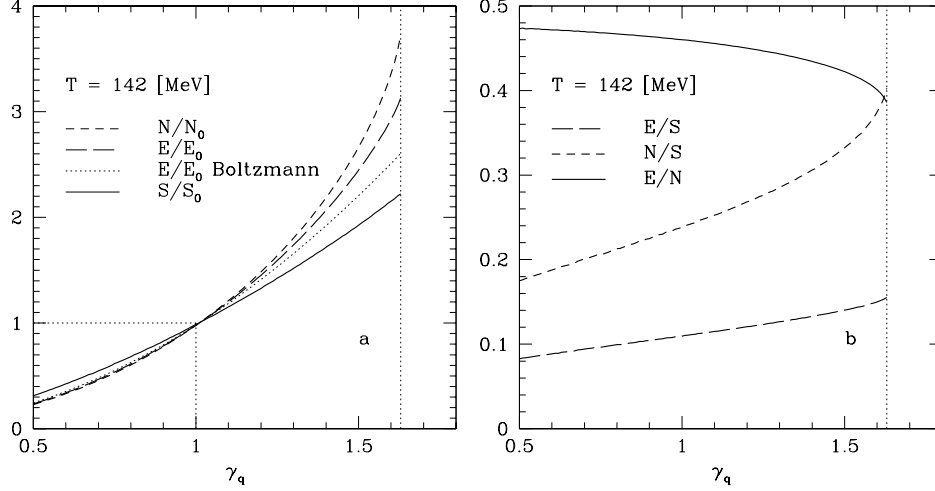


Fig. 2. Dependence of pion gas properties ( $N$ -particle,  $E$ -energy and  $S$ -entropy) density as function of  $\gamma_q$  for  $T = 142$  MeV. **a)** ratios relative to equilibrium value  $\gamma_q = 1$ ; **b)** relative ratios, thus  $E/N$ ,  $S/N$  and  $E/S$ .

into hadrons, without need for reheating, or a mixed phase which would allow the volume to grow. In short, the finding of the maximum allowable  $\gamma_q$  is intrinsically consistent with the notion of an explosively disintegrating QGP phase.

### 3. Update of SPS Experimental Data Analysis

In the past year our work addressed our discovery that consideration of the light quark chemical non-equilibrium is necessary in order to arrive at a consistent interpretation of the experimental results emanating from CERN [30]. We have also incorporated in our earlier analysis of the Pb–Pb system [5] a study of collective matter flow. Properties of the dense fireball as determined in this approach offer clear evidence that a QGP disintegrates at  $T_f \simeq 144$  MeV, corresponding to energy density  $\varepsilon = \mathcal{O}(0.5)$  GeV/fm<sup>3</sup> [31]. With flow, the analysis addresses also the  $m_\perp$ -slopes of strange particles. Notably, the near equality of (inverse) slopes of nearly all strange baryons and antibaryons arises by means of the sudden hadronization at the surface of an exploding QGP fireball. In the hadron based microscopic simulations this behavior of  $m_\perp$ -slopes can also arise allowing for particle-dependent freeze-out times [33].

We note that though we use six parameters to characterize the hadron phase space at chemical freeze-out, compare section 2, there are only two



truly unknown properties: the chemical freeze-out temperature  $T_f$  and the light quark fugacity  $\lambda_q$  (or equivalently, the baryochemical potential Eq. (4)) — we recall that the parameters  $\gamma_i$ ,  $i = q, s$  controls overall abundance of quark pairs, while  $\lambda_i$  controls the difference between quarks and anti-quarks of given flavor. As already noted earlier, the four other parameters are not arbitrary, and we could have used their tacit and/or computed values:

1) the strange quark fugacity  $\lambda_s$  is usually fixed by the requirement that strangeness balances  $\langle s - \bar{s} \rangle = 0$  [18]. The Coulomb distortion of the strange quark phase space plays an important role in the understanding of this constraint for Pb–Pb collisions, see Eq. (10) [5];

2) the strange quark phase space occupancy  $\gamma_s$  can be computed within the established kinetic theory framework for strangeness production [1, 23];

3) the tacitly assumed equilibrium phase space occupancy of light quarks  $\gamma_q = 1$ ;

4) assumed collective expansion to proceed at the relativistic sound velocity,  $v_c = 1/\sqrt{3}$  [1].

However, the rich particle data basis allows us to find from experiment the actual values of these four parameters, allowing to confront the theoretical results and/or hypothesis with experiment.

The value of  $\lambda_s$  we obtain from the strangeness conservation condition  $\langle s - \bar{s} \rangle = 0$  in QGP is, to a very good approximation [5]:

$$\tilde{\lambda}_s \equiv \lambda_s \lambda_Q^{1/3} = 1, \quad \lambda_Q \equiv \frac{\int_{R_f} d^3 r e^{\frac{V}{T}}}{\int_{R_f} d^3 r}. \quad (10)$$

$\lambda_Q < 1$  expresses the Coulomb deformation of strange quark phase space. This effect is relevant in central Pb–Pb interactions, but not in S–Au/W/Pb reactions.  $\lambda_Q$  is not a fugacity that can be adjusted to satisfy a chemical condition, since consideration of  $\lambda_i$ ,  $i = u, d, s$  exhausts all available chemical balance conditions for the abundances of hadronic particles. The subscript  $R_f$  in Eq. (10) reminds us that the classically allowed region within the dense matter fireball is included in the integration over the level density. Choosing  $R_f = 8$  fm,  $T = 140$  MeV,  $m_s = 200$  MeV (value of  $\gamma_s$  is practically irrelevant), for  $Z_f = 150$  the value is  $\lambda_s = 1.10$ .

The available compatible particle yield ratios (excluding  $\Omega$  and  $\bar{\Omega}$ , see section 1) are listed in table 1, top section from the experiment WA97 for  $p_\perp > 0.7$  GeV within a narrow  $\Delta y = 0.5$  central rapidity window. Further below are shown results from the large acceptance experiment NA49, extrapolated to full  $4\pi$  phase space coverage. We first fit 11 experimental results shown in table 1, and then turn to include also the  $m_\perp$ -slope in our

Table 1. WA97 (top) and NA49 (bottom) Pb–Pb 158A GeV particle ratios and some of our theoretical results, see text for explanation.

Ratios	Ref.	Exp.Data	Pb  <sub>0</sub>	Pb  <sub>v</sub>	Pb  <sub>v</sub> <sup>sb</sup>	Pb  <sub>v</sub> <sup>sc</sup>
$\Xi/\Lambda$	[13]	$0.099 \pm 0.008$	0.104	0.103	0.105	0.103
$\Xi/\bar{\Lambda}$	[13]	$0.203 \pm 0.024$	0.214	0.208	0.209	0.206
$\bar{\Lambda}/\Lambda$	[13]	$0.124 \pm 0.013$	0.124	0.125	0.124	0.125
$\Xi/\Xi$	[13]	$0.255 \pm 0.025$	0.256	0.252	0.248	0.251
$\frac{(\Xi+\Xi)}{(\Lambda+\Lambda)}$	[34]	$0.13 \pm 0.03$	0.126	0.122	0.124	0.122
$K_s^0/\phi$	[8]	$11.9 \pm 1.5$	14.2	13.3	13.0	13.4
$K^+/K^-$	[9]	$1.80 \pm 0.10$	1.80	1.82	1.78	1.83
$p/\bar{p}$	[7]	$18.1 \pm 4.$	17.3	16.7	16.6	16.6
$\Lambda/\bar{p}$	[35]	$3. \pm 1.$	2.68	2.11	2.11	2.11
$K_s^0/B$	[36]	$0.183 \pm 0.027$	0.181	0.181	0.163	0.188
$h^-/B$	[37]	$1.97 \pm 0.1$	1.96	1.97	1.97	1.96
$\chi_T^2$			3.6	2.5	3.2	2.6
$N; p; r$			11;5;2	12;6;2	12;5;2	12;5;2

considerations, and thus have 12 data points. The total error:

$$\chi_T^2 \equiv \frac{\sum_j (R_{\text{th}}^j - R_{\text{exp}}^j)^2}{(\Delta R_{\text{exp}}^j)^2} \quad (11)$$

for the four theoretical columns is shown at the bottom of this table along with the number of data points ‘ $N$ ’, parameters ‘ $p$ ’ used and (algebraic) redundancies ‘ $r$ ’ connecting the experimental results. For  $r \neq 0$  it is more appropriate to quote the total  $\chi_T^2$ , with a initial qualitative statistical relevance condition  $\chi_T^2/(N - p) < 1$ . The first theoretical columns refer to results without collective velocity  $v_c$  (subscript 0) the three other with fitted  $v_c$  (subscript  $v_c$ ). In column three, superscript ‘ $sb$ ’ means that  $\lambda_s$  is fixed by strangeness balance and, in column four, superscript ‘ $sc$ ’ means that  $\gamma_q = \gamma_q^c = e^{m_\pi/2T_f}$ , that is  $\gamma_q$  is fixed by its upper limit, the pion condensation point. All results have been newly recomputed, to account for slightly higher value of the ratio  $h^-/B$  [37].

It is interesting to note that the highest confidence result is obtained in the last column, just when the light quark phase space occupancy assumes value at the pion condensation point: here the number of degrees of freedom is higher than in the second column, obtained without constraint. It is unclear at present what is the full extent of this remarkable result. Another interesting insight is that radial flow always on its own improves our ability to describe the data. However,  $m_\perp$  spectra offer another independent measure of flow, and confirm very strongly our findings about the value of

Table 2. Experimental and theoretical  $m_\perp$  spectra inverse slopes  $T_{\text{th}}$ . Left Pb–Pb results from experiment NA49 [11] for kaons and from experiment WA97 [14] for baryons; right S–W results from WA85 [38].

	$T_\perp^{\text{Pb}}$ [MeV]	$T_{\text{th}}^{\text{Pb}}$ [MeV]	$T_\perp^{\text{S}}$ [MeV]	$T_{\text{th}}^{\text{S}}$ [MeV]
$T^{\text{K}^0}$	$223 \pm 13$	241	$219 \pm 5$	215
$T^\Lambda$	$291 \pm 18$	280	$233 \pm 3$	236
$T^{\bar{\Lambda}}$	$280 \pm 20$	280	$232 \pm 7$	236
$T^\Xi$	$289 \pm 12$	298	$244 \pm 12$	246
$T^{\Xi^-}$	$269 \pm 22$	298	$238 \pm 16$	246

$v_c$ . We proceeded as follows: for a given pair of values  $T_f$  and  $v_c$  we evaluate the resulting  $m_\perp$  particle spectrum and analyze it using the spectral shape and kinematic cuts employed by the experimental groups. To find the best values we consider just one ‘mean’ strange baryon experimental value  $\bar{T}_\perp^{\text{Pb}} = 260 \pm 10$ , since within the error the high  $m_\perp$  strange (anti)baryon inverse slopes are overlapping. Thus when considering  $v_c$  along with  $\bar{T}_\perp$  we have one parameter and one data point more. Once we find best values of  $T_f$  and  $v_c$ , we study again the inverse slopes of individual particle spectra. We obtain an acceptable agreement with the experimental  $T_\perp^j$  as shown in left section of table 2.

For comparison, we have also considered in the same framework the S-induced reactions, and the right section of table 2 shows a good agreement with the WA85 experimental data [38]. We used as the ‘mean’ experimental slope data point  $\bar{T}_\perp^{\text{S}} = 235 \pm 10$ . We can see that within a significantly smaller error bar, we obtained an accurate description of the  $m_\perp^{\text{S}}$ -slope data. This analysis implies that the kinetic freeze-out, where elastic particle-particle collisions cease, cannot be occurring at a condition very different from the chemical freeze-out. However, one pion HBT analysis at  $p_\perp < 0.5$  GeV suggests kinetic pion freeze-out at about  $T_k \simeq 120$  MeV [39]. A possible explanation of why here considered  $p_\perp > 0.7$  GeV particles are not subject to a greater spectral deformation after chemical freeze-out, is that they escape before the bulk of softer hadronic particles is formed. At least for strange baryons and antibaryons this is the result also seen in a recent microscopic study of the freeze-out process [22].

The six statistical parameters describing the particle abundances are shown in the top section of table 3, where we also show in the last column for comparison, the best result for S-induced reactions, where the target has been W/Au/Pb [4]. The errors in the results are one standard deviation errors arising from the propagation of the experimental measurement error, but apply only when the theoretical model describes the data well. All

Table 3. Heading:  $\chi^2_T$ , number of data points  $N$ , parameters  $p$  and redundancies  $r$ ; upper section: statistical model parameters which best describe the experimental results for Pb–Pb data, and in last column for S–Au/W/Pb data presented in Ref. [4]. Bottom section: specific energy, entropy, anti-strangeness, net strangeness of the full hadron phase space characterized by these statistical parameters. In column three we fix  $\lambda_s$  by requirement of strangeness conservation, and in column four we choose  $\gamma_q = \gamma_q^c$ , the pion condensation point.

	Pb  <sub>v</sub>	Pb  <sub>v</sub> <sup>sb</sup>	Pb  <sub>v</sub> <sup>sc</sup>	S  <sub>v</sub>
$\chi^2_T$ ; $N$ ; $p$ ; $r$	2.5; 12; 6; 2	3.2; 12; 5; 2	2.6; 12; 5; 2	6.2; 16; 6; 6
$T_f$ [MeV]	$142 \pm 3$	$144 \pm 2$	$142 \pm 2$	$144 \pm 2$
$v_c$	$0.54 \pm 0.04$	$0.54 \pm 0.025$	$0.54 \pm 0.025$	$0.49 \pm 0.02$
$\lambda_q$	$1.61 \pm 0.02$	$1.605 \pm 0.025$	$1.615 \pm 0.025$	$1.51 \pm 0.02$
$\lambda_s$	$1.09 \pm 0.02$	1.10*	$1.09 \pm 0.02$	$1.00 \pm 0.02$
$\gamma_q$	$1.7 \pm 0.5$	$1.8 \pm 0.2$	$\gamma_q^c = e^{m_\pi/2T_f}$	$1.41 \pm 0.08$
$\gamma_s/\gamma_q$	$0.79 \pm 0.05$	$0.80 \pm 0.05$	$0.79 \pm 0.05$	$0.69 \pm 0.03$
$E_f/B$	$7.8 \pm 0.5$	$7.7 \pm 0.5$	$7.8 \pm 0.5$	$8.2 \pm 0.5$
$S_f/B$	$42 \pm 3$	$41 \pm 3$	$43 \pm 3$	$44 \pm 3$
$s_f/B$	$0.69 \pm 0.04$	$0.67 \pm 0.05$	$0.70 \pm 0.05$	$0.73 \pm 0.05$
$(\bar{s}_f - s_f)/B$	$0.03 \pm 0.04$	0*	$0.04 \pm 0.05$	$0.17 \pm 0.05$

results shown in table 3 have convincing statistical confidence level. For the S-induced reactions the number of redundancies  $r$  shown in heading of the table 3 is large, since same data comprising different kinematic cuts has been included in the analysis. It is quite reassuring that within error the freeze-out temperature  $T_f$  seen in table 3, is the same for both the S- and Pb-induced reactions, even though the chemical phase space occupancies differ greatly. This must be the case within our model of sudden freeze-out and constitutes its firm confirmation. The variation in the shape of the particle spectra is fully explained by a change in the collective velocity, which rises from  $v_c^S = 0.49 \pm 0.02$  to  $v_c^{\text{Pb}} = 0.54 \pm 0.04 \simeq 1/\sqrt{3} = 0.577$ . The light quark fugacity  $\lambda_q$  implies that baryochemical potential is  $\mu_B^{\text{Pb}} = 203 \pm 5 > \mu_B^S = 178 \pm 5$  MeV. As in S-induced reactions where  $\lambda_s = 1$ , now in Pb-induced reactions, a value  $\lambda_s^{\text{Pb}} \simeq 1.1$  characteristic for a source of freely movable strange quarks with balancing strangeness, *i.e.*,  $\tilde{\lambda}_s = 1$  is obtained, see Eq. (10).

The values of  $\gamma_q > 1$ , seen in table 3, imply that there is phase space over-abundance of light quarks, to which, *e.g.*, gluon fragmentation at QGP breakup *prior* to hadron formation contributes.  $\gamma_q$  assumes in our data analysis a value near to where pions could begin to condense [30], Eq. (2). We found studying the ratio  $h^-/B$  separately from other experimental results that the value of  $\gamma_q \simeq \gamma_q^c$  is fixed consistently and independently both, by

the negative hadron ( $h^-$ ), and the strange hadron yields. The unphysical range  $\gamma_q > \gamma_q^c \simeq 1.63$  can arise (see column Pb| $v$ <sup>Sb</sup>) since, up to this point, we use only a first quantum (Bose/Fermi) correction. However, when Bose distribution for pions is implemented, which requires the constraint  $\gamma_q \leq \gamma_q^c$ , we obtain practically the same results, as shown in second column of table 3. We then show in table 3 the ratio  $\gamma_s/\gamma_q \simeq 0.8$ , which corresponds (approximately) to the parameter  $\gamma_s$  when  $\gamma_q = 1$  had been assumed. We note that  $\gamma_s^{\text{Pb}} > 1$ . This strangeness over-saturation effect could arise from the effect of gluon fragmentation combined with early chemical equilibration in QGP,  $\gamma_s(t < t_f) \simeq 1$ . The ensuing rapid expansion preserves this high strangeness yield, and thus we find the result  $\gamma_s > 1$ , as is shown in Fig. 33 in [1].

We show, in the bottom section of table 3, the energy and entropy content per baryon, and specific anti-strangeness content, along with specific strangeness asymmetry of the hadronic particles emitted. The energy per baryon seen in the emitted hadrons is nearly equal to the available specific energy of the collision (8.6 GeV for Pb–Pb, 8.8–9 GeV for S–Au/W/Pb). This implies that the fraction of energy deposited in the central fireball must be nearly the same as the fraction of baryon number. The small reduction of the specific entropy in Pb–Pb compared to the lighter S–Au/W/Pb system maybe driven by the greater baryon stopping in the larger system, also seen in the smaller energy per baryon content. Both collision systems freeze out at energy per unit of entropy  $E/S = 0.185$  GeV. There is a loose relation of this universality in the chemical freeze-out condition with the suggestion made recently that particle freeze-out occurs at a fixed energy per baryon for all physical systems [40], since the entropy content is related to particle multiplicity. The overall high specific entropy content we find agrees well with the entropy content evaluation made earlier [27] for the S–W case.

Inspecting Fig. 38 in [1], we see that the specific yield of strangeness we expect from the kinetic theory in QGP is at the level of 0.75 per baryon, in agreement with the results of present analysis shown in table 3. This high strangeness yield leads to the enhancement of multi-strange (anti)baryons, which are viewed as important hadronic signals of QGP phenomena [41], and a series of recent experimental analysis has carefully demonstrated comparing p–A with A–A results that there is quite significant enhancement [14, 42], as has also been noted before by the experiment NA35 [43]. The strangeness imbalance seen in the asymmetrical S–Au/W/Pb system (bottom of table 3) could be a real effect arising from hadron phase space properties. However, this result also reminds us that though the statistical errors are very small, there could be in this asymmetric system a considerable systematic error due to presence of a significant spectator matter component. In the symmetric Pb–Pb collisions this effect disappears, despite the fact that the freeze-out flow pattern could be much more complex and there

could be a distortion of particle spectra at low momenta not accounted for in our study, for we did not model the ratio of kaons to hyperons. Considering this limitation it is indeed remarkable, how well the conservation of strangeness condition is satisfied, when it is not being enforced.

#### 4. RHIC and Dynamics of Strangeness Production

In some key aspects, the methods to describe strangeness production which we have been developing differ from those obtained in other studies of chemical equilibration of quark flavor, in particular for RHIC conditions [44, 45, 46]. For example, we use running QCD parameters (both coupling and strange quark mass) with strong coupling constant  $\alpha_s$  as determined at the  $M_{Z^0}$  energy scale. We also incorporate entropy conserving flow into the dynamical equations directly, exploiting significant cancellations that occur, and thus obtain a relatively simple dynamical model for the evolution of the phase space occupancy  $\gamma_s$  of strange quarks in the expanding QGP.

The phase space distribution  $f_s$  can be characterized by a local temperature  $T(\vec{x}, t)$  of a (Boltzmann) equilibrium distribution  $f_s^\infty$ , with normalization set by a phase space occupancy factor:

$$f_s(\vec{p}, \vec{x}; t) \simeq \gamma_s(T) f_s^\infty(\vec{p}; T). \quad (12)$$

Eq. (12) invokes in the momentum independence of  $\gamma_s$  our first assumption. More generally, the factor  $\gamma_i$ ,  $i = g, q, s, c$ , allows a local density of gluons, light quarks, strange quarks and charmed quarks, respectively not to be determined by the local momentum shape, but to evolve independently. With variables  $(t, \vec{x})$  referring to an observer in the laboratory frame, the chemical evolution can be described by the strange quark current non-conservation arising from strange quark pair production described by a Boltzmann collision term:

$$\begin{aligned} \partial_\mu j_s^\mu \equiv \frac{\partial \rho_s}{\partial t} + \frac{\partial \vec{v} \rho_s}{\partial \vec{x}} = & \frac{1}{2} \rho_g^2(t) \langle \sigma v \rangle_T^{gg \rightarrow s\bar{s}} \\ & + \rho_q(t) \rho_{\bar{q}}(t) \langle \sigma v \rangle_T^{q\bar{q} \rightarrow s\bar{s}} - \rho_s(t) \rho_{\bar{s}}(t) \langle \sigma v \rangle_T^{s\bar{s} \rightarrow gg, q\bar{q}}. \end{aligned} \quad (13)$$

The factor 1/2 avoids double counting of gluon pairs. The implicit sums over spin, color and any other discrete quantum numbers are combined in the particle density  $\rho = \sum_{s,c,\dots} \int d^3p f$ , and we have also introduced the momentum averaged production/annihilation thermal reactivities (also called ‘rate coefficients’):

$$\langle \sigma v_{\text{rel}} \rangle_T \equiv \frac{\int d^3p_1 \int d^3p_2 \sigma_{12} v_{12} f(\vec{p}_1, T) f(\vec{p}_2, T)}{\int d^3p_1 \int d^3p_2 f(\vec{p}_1, T) f(\vec{p}_2, T)}. \quad (14)$$

$f(\vec{p}_i, T)$  are the relativistic Boltzmann/Jüttner distributions of two colliding particles  $i = 1, 2$  of momentum  $p_i$ .

The current conservation used above in the laboratory ‘Eulerian’ formulation can also be written with reference to the individual particle dynamics in the so called ‘Lagrangian’ description: consider  $\rho_s$  as the inverse of the small volume available to each particle. Such a volume is defined in the local frame of reference for which the local flow vector vanishes  $\vec{v}(\vec{x}, t)|_{\text{local}} = 0$ . The considered volume  $\delta V_l$  being occupied by small number of particles  $\delta N$  (*e.g.*,  $\delta N = 1$ ), we have:

$$\delta N_s \equiv \rho_s \delta V_l. \quad (15)$$

The left hand side (LHS) of Eq. (13) can be now written as:

$$\frac{\partial \rho_s}{\partial t} + \frac{\partial \vec{v} \rho_s}{\partial \vec{x}} \equiv \frac{1}{\delta V_l} \frac{d \delta N_s}{dt} = \frac{d \rho_s}{dt} + \rho_s \frac{1}{\delta V_l} \frac{d \delta V_l}{dt}. \quad (16)$$

Since  $\delta N$  and  $\delta V_l dt$  are L(orentz)-invariant, the actual choice of the frame of reference in which the right hand side (RHS) of Eq. (16) is studied is irrelevant and we drop henceforth the subscript  $l$ .

We can further adapt Eq. (16) to the dynamics we pursue: we introduce  $\rho_s^\infty(T)$  as the (local) chemical equilibrium abundance of strange quarks, thus  $\rho = \gamma_s \rho_s^\infty$ . We evaluate the equilibrium abundance  $\delta N_s^\infty = \delta V \rho_s^\infty(T)$  integrating the Boltzmann distribution:

$$\delta N_s^\infty = [\delta V T^3] \frac{3}{\pi^2} z^2 K_2(z), \quad z = \frac{m_s}{T}, \quad (17)$$

where  $K_\nu$  is the modified Bessel function of order  $\nu$ ; we will below use:  $d[z^\nu K_\nu(z)]/dz = -z^\nu K_{\nu-1}$ . The first factor on the RHS in Eq. (17) is a constant in time should the evolution of matter after the initial pre-thermal time period  $\tau_0$  be entropy conserving [47], and thus  $\delta V T^3 = \delta V_0 T_0^3 = \text{Const.}$ . We now substitute in Eq. (16) and obtain

$$\frac{\partial \rho_s}{\partial t} + \frac{\partial \vec{v} \rho_s}{\partial \vec{x}} = \dot{T} \rho_s^\infty \left( \frac{d \gamma_s}{dT} + \frac{\gamma_s}{T} z \frac{K_1(z)}{K_2(z)} \right), \quad (18)$$

where  $\dot{T} = dT/dt$ . Note that in Eq. (18) only a part of the usual flow-dilution term is left, since we implemented the adiabatic volume expansion, and study the evolution of the phase space occupancy in lieu of particle density. The dynamics of the local temperature is the only quantity we need to model.

We now return to study the collision terms seen on the RHS of Eq. (13). A related quantity is the (L-invariant) production rate  $A^{12 \rightarrow 34}$  of particles

per unit time and space, defined usually with respect to chemically equilibrated distributions:

$$A^{12 \rightarrow 34} \equiv \frac{1}{1 + \delta_{1,2}} \rho_1^\infty \rho_2^\infty \langle \sigma_s v_{12} \rangle_T^{12 \rightarrow 34}. \quad (19)$$

The factor  $1/(1 + \delta_{1,2})$  is introduced to compensate double-counting of identical particle pairs. In terms of the L-invariant  $A$ , Eq. (13) takes the form:

$$\begin{aligned} \dot{T} \rho_s^\infty \left( \frac{d\gamma_s}{dT} + \frac{\gamma_s}{T} z \frac{K_1(z)}{K_2(z)} \right) &= \gamma_g^2(\tau) A^{gg \rightarrow s\bar{s}} + \\ &+ \gamma_q(\tau) \gamma_{\bar{q}}(\tau) A^{q\bar{q} \rightarrow s\bar{s}} - \gamma_s(\tau) \gamma_{\bar{s}}(\tau) (A^{s\bar{s} \rightarrow gg} + A^{s\bar{s} \rightarrow q\bar{q}}). \end{aligned} \quad (20)$$

Only weak interactions convert quark flavors, thus, on hadronic time scale, we have  $\gamma_{s,q}(\tau) = \gamma_{\bar{s},\bar{q}}(\tau)$ . Moreover, detailed balance, arising from the time reversal symmetry of the microscopic reactions, assures that the invariant rates for forward/backward reactions are the same, specifically

$$A^{12 \rightarrow 34} = A^{34 \rightarrow 12}, \quad (21)$$

and thus:

$$\begin{aligned} \dot{T} \rho_s^\infty \left( \frac{d\gamma_s}{dT} + \frac{\gamma_s}{T} z \frac{K_1(z)}{K_2(z)} \right) &= \gamma_g^2(\tau) A^{gg \rightarrow s\bar{s}} \left[ 1 - \frac{\gamma_s^2(\tau)}{\gamma_q^2(\tau)} \right] \\ &+ \gamma_q^2(\tau) A^{q\bar{q} \rightarrow s\bar{s}} \left[ 1 - \frac{\gamma_s^2(\tau)}{\gamma_q^2(\tau)} \right]. \end{aligned} \quad (22)$$

When all  $\gamma_i \rightarrow 1$ , the Boltzmann collision term vanishes, we have reached equilibrium.

As discussed, the gluon chemical equilibrium is thought to be reached at high temperatures well before the strangeness equilibrates chemically, and thus we assume this in what follows, and the initial conditions we will study refer to the time at which gluons are chemically equilibrated. Setting  $\lambda_g = 1$  (and without a significant further consequence for what follows, since gluons dominate the production rate, also  $\lambda_q = 1$ ) we obtain after a straightforward manipulation the dynamical equation describing the evolution of the local phase space occupancy of strangeness:

$$2\tau_s \dot{T} \left( \frac{d\gamma_s}{dT} + \frac{\gamma_s}{T} z \frac{K_1(z)}{K_2(z)} \right) = 1 - \gamma_s^2. \quad (23)$$

Here, we defined the relaxation time  $\tau_s$  of chemical (strangeness) equilibration as the ratio of the equilibrium density that is being approached, with the rate at which this occurs:

$$\tau_s \equiv \frac{1}{2} \frac{\rho_s^\infty}{(A^{gg \rightarrow s\bar{s}} + A^{q\bar{q} \rightarrow s\bar{s}} + \dots)}. \quad (24)$$



The factor  $1/2$  is introduced by convention in order for the quantity  $\tau_s$  to describe the exponential approach to equilibrium.

Eq. (23) is our final analytical result describing the evolution of phase space occupancy. Since one generally expects that  $\gamma_s \rightarrow 1$  in a monotonic fashion as function of time, it is important to appreciate that this equation allows  $\gamma_s > 1$ : when  $T$  drops below  $m_s$ , and  $1/\tau_s$  becomes small, the dilution term (2nd term on LHS) in Eq. (23) dominates the evolution of  $\gamma_s$ . In simple terms, the high abundance of strangeness produced at high temperature over-populates the available phase space at lower temperature, when the equilibration rate cannot keep up with the expansion cooling. This behavior of  $\gamma_s$  has been shown in [32, Fig. 2] for the SPS conditions with fast transverse expansion. Since we assume that the dynamics of transverse expansion of QGP is similar at RHIC as at SPS, we will obtain a rather similar behavior for  $\gamma_s$ . We note that yet a faster transverse expansion than considered here could enhance the chemical strangeness anomaly.

$\tau_s(T)$ , Eq. (24), has been evaluated using pQCD cross section and employing NLO (next to leading order) running of both the strange quark mass and QCD-coupling constant  $\alpha_s$  [48]. We believe that this method produces a result for  $\alpha_s$  that can be trusted down to 1 GeV energy scale which is here relevant. We employ results obtained with  $\alpha_s(M_{Z^0}) = 0.118$  and  $m_s(1\text{GeV}) = 200\text{ MeV}$ ; we have shown results with  $m_s(1\text{GeV}) = 220\text{ MeV}$  earlier [2]. There is some systematic uncertainty due to the appearance of the strange quark mass as a fixed rather than running value in both, the chemical equilibrium density  $\rho_s^\infty$  in Eq. (24), and in the dilution term in Eq. (23). We use the value  $m_s(1\text{ GeV})$ , with the 1 GeV energy scale chosen to correspond to typical interaction scale in the QGP at temperatures under consideration.

## 5. Expectations for Strange Hadron Production at RHIC

We now combine our advances in theoretical models of strangeness production and data interpretation at SPS energies with the objective of making reliable predictions for the RHIC energy range [2]. First we address the question how much strangeness can be expected at RHIC. Numerical study of Eq. (23) becomes possible as soon as we define the temporal evolution of the temperature for RHIC conditions. We expect that a global cylindrical expansion should describe the dynamics: aside of the longitudinal flow, we allow the cylinder surface to expand given the internal thermal pressure. SPS experience suggests that the transverse matter flow will not exceed the sound velocity of relativistic matter  $v_\perp \simeq c/\sqrt{3}$ . We recall that for pure longitudinal expansion local entropy density scales as  $S \propto T^3 \propto 1/\tau$ , [47]. It is likely that the transverse flow of matter will accelerate the drop in en-

tropy density. We thus consider the following temporal evolution function of the temperature:

$$T(\tau) = T_0 \left[ \frac{1}{(1 + \tau \, 2c/d)(1 + \tau \, v_{\perp}/R_{\perp})^2} \right]^{1/3}. \quad (25)$$

We take the thickness of the initial collision region at  $T_0 = 0.5 \text{ GeV}$  to be  $d(T_0 = 0.5)/2 = 0.75 \text{ fm}$ , and the transverse dimension in nearly central Au–Au collisions to be  $R_{\perp} = 4.5 \text{ fm}$ . The time at which thermal initial conditions are reached is assumed to be  $\tau_0 = 1 \text{ fm}/c$ . When we vary  $T_0$ , the temperature at which the gluon equilibrium is reached, we also scale the longitudinal dimension according to:

$$d(T_0) = (0.5 \text{ GeV}/T_0)^3 1.5 \text{ fm}. \quad (26)$$

This assures that when comparing the different evolutions of  $\gamma_s$  we are looking at an initial system that has the same entropy content by adjusting its initial volume  $V_0$ . The reason we vary the initial temperature  $T_0$  down to 300 MeV, maintaining the initial entropy content is to understand how the assumption about the chemical equilibrium of gluons, reached by definition at  $T_0$ , impacts our result. In fact when considering decreasing  $T_0$  (and thus increasing  $V_0$ ), what we are doing is to begin the thermal production at a later time in the history of the collision.

The numerical integration of Eq. (23) is started at  $\tau_0$ , and a range of initial temperatures  $300 \leq T_0 \leq 600$ , varying in steps of 50 MeV. The high limit of the temperature we explore exceeds somewhat the ‘hot glue scenario’ [19], while the lower limit of  $T_0$  corresponds to the more conservative estimates of possible initial conditions [47]. Since the initial  $p$ – $p$  collisions also produce strangeness, we take as an estimate of initial abundance a common initial value  $\gamma_s(T_0) = 0.15$ . The time evolution in the plasma phase is followed up to the break-up of QGP. This condition we establish in view of our analysis of the SPS results. We recall that SPS-analysis showed that the system dependent baryon and antibaryon  $m_{\perp}$ -slopes of particle spectra are result of differences in collective flow in the deconfined QGP source at freeze-out. There is a universality of physical properties of hadron chemical freeze-out between different SPS systems, and in our analysis a practical coincidence of the kinetic freeze-out conditions with the chemical freeze-out. We thus expect, extrapolating the phase boundary curve to the small baryochemical potentials, that the QGP break-up temperature  $T_f^{\text{SPS}} \simeq 145 \pm 5 \text{ MeV}$  will see just a minor upward change to the value  $T_f^{\text{RHIC}} \simeq 150 \pm 5 \text{ MeV}$ .

With the freeze-out condition fixed, one would think that the major uncertainty in our approach comes from the initial gluon equilibration temperature  $T_0$ , and we now study how different values of  $T_0$  influence the final

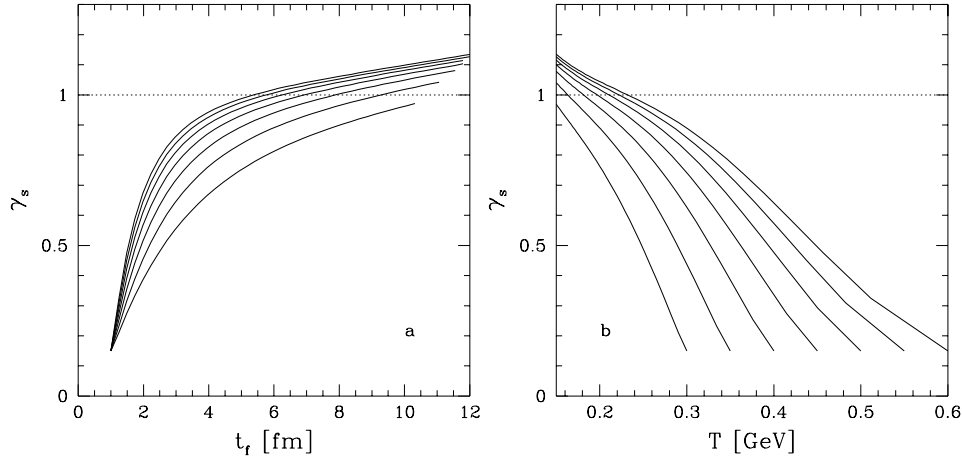


Fig. 3. Evolution of QGP-phase strangeness phase space occupancy  $\gamma_s$ . **a)** as function of time and, **b)** as function of temperature for  $m_s(1 \text{ GeV}) = 200 \text{ MeV}$ , see text for details.

state phase space occupancy. We integrate numerically Eq. (23) and present  $\gamma_s$  as function of both time  $t$  in Fig. 3a, and temperature  $T$  in Fig. 3b, up to the expected QGP breakup at  $T_f^{\text{RHIC}} \simeq 150 \pm 5 \text{ MeV}$ . We see that:

- widely different initial conditions (with similar initial entropy content) lead to rather similar chemical conditions at chemical freeze-out of strangeness,
- despite a series of conservative assumptions, we find, not only, that strangeness equilibrates, but indeed that the dilution effect allows an overpopulation of the strange quark phase space. For a wide range of initial conditions, we obtain a narrow band  $1.15 > \gamma_s(T_f) > 1$ . We will in the following, taking into account some contribution from hadronization of gluons in strange/antistrange quarks, adopt what the value  $\gamma_s(T_f) = 1.25$ .

We now consider how this relatively large value of  $\gamma_s$ , characteristic for the underlying QGP formation and evolution of strangeness, impacts the strange baryon and anti-baryon observable emerging in hadronization. Remembering that major changes compared to SPS should occur in rapidity spectra of mesons, baryons and antibaryons, we will apply the same hadronization model that worked in the analysis of the SPS data. This hypothesis can be falsified easily, since we expect, based and compared to the Pb–Pb 158A GeV results:

- a) shape identity of all RHIC  $m_\perp$  and  $y$  spectra of antibaryons  $\bar{p}$ ,  $\bar{\Lambda}$ ,  $\bar{\Xi}$ , since in our approach there is no difference in their production mechanism, and the form of the spectra is determined in a similar way by the local temperature and flow velocity vector;

b) the  $m_{\perp}$ -slopes of these antibaryons should be very similar to the result we have from Pb–Pb 158A GeV since only a slight increase in the freeze-out temperature occurs, and no increase in collective transverse flow is expected.

The abundances of particles produced from QGP within the sudden freeze-out model are controlled by several parameters we addressed earlier: the light quark fugacity  $1 < \lambda_q < 1.1$ , value is limited by the expected small ratio between baryons and mesons (baryon-poor plasma) when the energy per baryon is above 100 GeV, strangeness fugacity  $\lambda_s \simeq 1$  which value for locally neutral plasma assures that  $\langle s - \bar{s} \rangle = 0$ ; the light quark phase space occupancy  $\gamma_q \simeq 1.5$ , overabundance value due to gluon fragmentation. Given these narrow ranges of chemical parameters and the freeze-out temperature  $T_f = 150$  MeV, we compute the expected particle production at break-up. In general we cannot expect that the absolute numbers of particles we find are correct, as we have not modeled the important effect of flow in the laboratory frame of reference. However, ratios of hadrons subject to similar flow effects (compatible hadrons) can be independent of the detailed final state dynamics, as the results seen at SPS suggest, and we will look at such ratios more closely.

Taking  $\gamma_q = 1.5^{+0.10}_{-0.25}$  we choose the value of  $\lambda_q$ , see the header of table 4, for which the energy per baryon ( $E/B$ ) is similar to the collision condition (100 GeV), which leads to the range  $\lambda_q = 1.03 \pm 0.005$ . We evaluate for these examples aside of  $E/B$ , the strangeness per baryon  $s/B$  and entropy per baryon  $S/B$  as shown in the top section of the table 4. We do not enforce  $\langle s - \bar{s} \rangle = 0$  exactly, but since baryon asymmetry is small, strangeness is balanced to better than 2% in the parameter range considered. In the bottom portion of table 4, we present the compatible particle abundance ratios, computed according to the procedure developed in section 2. We have given, aside of the baryon and antibaryon relative yields, also the relative kaon yield, which is also well determined within our approach.

The meaning of these results can be better appreciated when we assume in an example the central rapidity density of direct protons is  $dp/dy|_{\text{cent.}} = 25$ . In table 5, we present the resulting (anti)baryon abundances. We see that the net baryon density  $db/dy \simeq 16 \pm 3$ , there is baryon number transparency. We see that (anti)hyperons are indeed more abundant than non-strange (anti)baryons. Taking into account the disintegration of strange baryons, we are finding a much greater number of observed protons  $dp/dy|_{\text{cent.}}^{\text{obs.}} \simeq 65 \pm 5$  in the central rapidity region. It is important when quoting results from table 5 to recall that:

- 1) we have chosen arbitrarily the overall normalization in table 5, only particle ratios were computed, and
- 2) the rapidity baryon density relation to rapidity proton density is a

Table 4. For  $\gamma_s = 1.25$ ,  $\lambda_s = 1$  and  $\gamma_q, \lambda_q$  as shown: Top portion: strangeness per baryon  $s/B$ , energy per baryon  $E/B[\text{GeV}]$  and entropy per baryon  $S/B$ . Bottom portion: sample of hadron ratios expected at RHIC.

$\gamma_q$	1.25	1.5	1.5	1.5	1.60
$\lambda_q$	1.03	1.025	1.03	1.035	1.03
$E/B[\text{GeV}]$	117	133	111	95	110
$s/B$	18	16	13	12	12
$S/B$	630	698	583	501	571
$p/\bar{p}$	1.19	1.15	1.19	1.22	1.19
$\Lambda/p$	1.74	1.47	1.47	1.45	1.35
$\bar{\Lambda}/\bar{p}$	1.85	1.54	1.55	1.55	1.44
$\bar{\Lambda}/\Lambda$	0.89	0.91	0.89	0.87	0.89
$\Xi^-/\Lambda$	0.19	0.16	0.16	0.16	0.15
$\bar{\Xi}^-/\bar{\Lambda}$	0.20	0.17	0.17	0.17	0.16
$\Xi/\Xi$	0.94	0.95	0.94	0.93	0.94
$\Omega/\Xi^-$	0.147	0.123	0.122	0.122	0.115
$\bar{\Omega}/\bar{\Xi}^-$	0.156	0.130	0.130	0.131	0.122
$\bar{\Omega}/\Omega$	1	1.	1.	1.	1.
$\frac{\Omega+\bar{\Omega}}{\Xi^-+\bar{\Xi}^-}$	0.15	0.13	0.13	0.13	0.12
$\frac{\Xi^-+\bar{\Xi}^-}{\Lambda+\bar{\Lambda}}$	0.19	0.16	0.16	0.16	0.15
$K^+/K^-$	1.05	1.04	1.05	1.06	1.05

Table 5.  $dN/dy|_{\text{cent.}}$  assuming in this example  $dp/dy|_{\text{cent.}} = 25$ .

$\gamma_q$	$\lambda_q$	$b$	$p$	$\bar{p}$	$\Lambda+\Sigma^0$	$\bar{\Lambda}+\bar{\Sigma}^0$	$\Sigma^\pm$	$\bar{\Sigma}^\mp$	$\Xi^0$	$\bar{\Xi}^0$	$\Omega=\bar{\Omega}$
1.25	1.03	17	25*	21	44	39	31	27	17	16	1.2
1.5	1.025	13	25*	22	36	33	26	23	13	11	0.7
1.5	1.03	16	25*	21	37	33	26	23	12	11	0.7
1.5	1.035	18	25*	21	36	32	26	22	11	10	0.7
1.60	1.03	15	25*	21	34	30	24	21	10	9.6	0.6

consequence of the assumed value of  $\lambda_q$ , which we chose to get  $E/B \simeq 100$  GeV per participant.

The most interesting result seen in table 5, the hyperon-dominance of the baryon yields at RHIC, does not depend on detailed model hypothesis. We have explored another set of parameters in our first and preliminary report on this matter [49], finding this result. Another interesting property of the hadronizing hot RHIC matter as seen in table 4, is that strangeness yield per participant is expected to be 13–23 times greater than seen at present at SPS energies, where we have 0.75 strange quark pairs per baryon. As seen in table 5, the baryon rapidity density is in our examples similar to the proton rapidity density.

## 6. Conclusions

We believe that the Fermi model interpretation of SPS strangeness results decisively shows some interesting new physics. We see considerable convergence of the results around properties of suddenly hadronizing QGP. The key results we obtained are:

- 1) same hadronization temperature  $T=142-144$  MeV for very different collision systems with different hadron spectra;
- 2) QGP expected  $\tilde{\lambda}_s = 1$  for S and Pb collisions, and  $\lambda_s^{\text{Pb}} \simeq 1.1$ ;
- 3)  $\gamma_s^{\text{Pb}} > 1$ , indicating that high strangeness yield was reached before freeze-out;
- 4)  $\gamma_q > 1$  as would be expected from high entropy phase and the associated value  $S/B \simeq 40$ ;
- 5) yield of strangeness per baryon  $\bar{s}/B \simeq 0.75$  just as predicted by gluon fusion in thermal QGP;
- 6) transverse expansion velocity  $v_c^{\text{Pb}} = 1/\sqrt{3}$ , the sound velocity of quark matter for Pb-Pb.

Among other interesting results which also verify the consistency of our approach, we recall:

- the exact balancing of strangeness  $\langle \bar{s} - s \rangle = 0$  in the symmetric Pb-Pb case;
- increase of the baryochemical potential  $\mu_B^{\text{Pb}} = 203 \pm 5 > \mu_B^{\text{S}} = 178 \pm 5$  MeV as the collision system grows;
- energy per baryon near to the value expected if energy and baryon number deposition in the fireball are similar.

The universality of the physical properties at chemical freeze-out for S- and Pb-induced reactions points to a common nature of the primordial source of hadronic particles. The difference in spectra between the two systems arises in our analysis due to the difference in the collective surface explosion velocity,  $v_c^{\text{S}} = 0.5 < v_c^{\text{Pb}} = 1/\sqrt{3}$ , which for larger system is higher, having more time to develop.

In our opinion, these results show that hadronic particles seen at CERN-SPS are emerging from a deconfined QGP phase of hadronic matter and do not undergo a re-equilibration after they have been produced. This has encouraged us to consider within the same computational scheme the production of strange hadrons at RHIC conditions, and we have shown that one can expect strangeness chemical equilibration in nuclear collisions at RHIC if the deconfined QGP is formed, with a probable overpopulation effect associated with the early strangeness abundance freeze-out before hadronization. We have shown also that (anti)hyperons dominate (anti)baryon abundance, and that rapidity distributions of (anti)protons are primarily deriving from decays of (anti)hyperons.

## REFERENCES

- [1] J. Rafelski, J. Letessier and A. Tounsi, *Acta Phys. Pol. B* **27**, 1035 (1996), and references therein.
- [2] Expected Production of Strange Baryons and Antibaryons in Baryon-Poor QGP, J. Rafelski and J. Letessier, nucl-th/9908024, to be published in *Phys. Lett. B* (1999)
- [3] E. Fermi, *Progr. Theor. Phys.* **5** 570 (1950); *Phys. Rev.* **81**, 115 (1950); *Phys. Rev.* **92**, 452 (1953).
- [4] J. Letessier and J. Rafelski, *Phys. Rev. C* **59**, 947 (1999).
- [5] J. Letessier and J. Rafelski, *Acta Phys. Pol. B* **30**, 153 (1999); *J. Phys. Part. Nucl.* **G25**, 295, (1999) .
- [6] J. Rafelski and J. Letessier, e-Print Archive: nucl-th/9903018.
- [7] G.J. Odyniec, *Nucl. Phys. A* **638**, 135, (1998).
- [8] F. Pühlhofer, NA49, *Nucl. Phys. A* **638**, 431, (1998).
- [9] C. Bormann, NA49, *J. Phys. G* **23**, 1817 (1997).
- [10] H. Appelshäuser *et al.*, NA49, *Phys. Lett. B* **444**, 523, (1998).
- [11] S. Margetis, NA49, *J. Physics G* **25**, 189 (1999).
- [12] A.K. Holme, WA97, *J. Phys. G* **23**, 1851 (1997).
- [13] I. Králik, WA97, *Nucl. Phys. A* **638**, 115, (1998).
- [14] E. Andersen *et al.*, WA97, *Phys. Lett. B* **433**, 209, (1998); **449**, 401 (1999).
- [15] J. Letessier, J. Rafelski and A. Tounsi, *Phys. Lett. B* **410**, 315 (1997).
- [16] F. Becattini, M. Gazdzicki and J. Sollfrank, *Eur. Phys. J. C* **5**, 143, (1998).
- [17] P. Koch, B. Müller and J. Rafelski, *Phys. Rep.* **142**, 167 (1986).
- [18] J. Rafelski, *Phys. Lett. B* **262**, 333 (1991); *Nucl. Phys. A* **544**, 279c (1992).
- [19] E. Shuryak, *Phys. Rev. Lett.* **68**, 3270 (1992).
- [20] Jan-e Alam, S. Raha and B. Sinha, *Phys. Rev. Lett.* **73**, 1895 (1994); P. Roy, Jan-e Alam, S. Sarkar, B. Sinha, and S. Raha, *Nucl. Phys. A* **624**, 687 (1997).
- [21] S.M.H. Wong *Phys. Rev. C* **56**, 1075 (1997).
- [22] A. Dumitru, S.A. Bass, M. Bleicher, H. Stöcker and W. Greiner *Phys. Lett. B* **460**, 411 (1999).
- [23] J. Rafelski and B. Müller, *Phys. Rev. Lett* **48**, 1066 (1982); **56**, 2334E (1986); P. Koch, B. Müller and J. Rafelski, *Z. Phys. A* **324**, 453 (1986).
- [24] T. Matsui, B. Svetitsky and L.D. McLerran, *Phys. Rev. D* **34**, 783 and 2047 (1986).
- [25] N. Bilic, J. Cleymans, I. Dadić and D. Hislop, *Phys. Rev. C* **52**, 401 (1995).
- [26] P. Koch and J. Rafelski, *Nucl. Phys. A* **444**, 678 (1985).
- [27] J. Letessier, A. Tounsi, U. Heinz, J. Sollfrank and J. Rafelski *Phys. Rev. Lett.* **70**, 3530 (1993); *Phys. Rev. D* **51**, 3408 (1995).

- [28] J. Letessier, A. Tounsi and J. Rafelski, *Phys. Rev. C* **50**, 406 (1994); [hep-ph/9711346];  
J. Rafelski, J. Letessier and A. Tounsi, *Acta Phys. Pol. A* **85**, 699 (1994).
- [29] E. Schnedermann, J. Sollfrank and U. Heinz, pp175–206 in *Particle Production in Highly Excited Matter*, NATO-ASI Series B303, H.H. Gutbrod and J. Rafelski, Eds., (Plenum, New York, 1993)
- [30] J. Rafelski and J. Letessier, nucl-th/9903018
- [31] F. Karsch, and M. Lütgemeier, *Nucl. Phys. B* **550**, 449 (1999).
- [32] J. Letessier, A. Tounsi and J. Rafelski, *Phys. Lett. B* **390**, 363 (1997).
- [33] H. van Hecke, H. Sorge and N. Xu, *Phys. Rev. Lett.* **81**, 5764 (1998).
- [34] G.J. Odyniec, for the NA49 Collaboration, *J. Phys. G* **23**, 1827 (1997).
- [35] D. Röhrig, for the NA49 Collaboration, “Recent results from NA49 experiment on Pb–Pb collisions at 158 A GeV”, see Fig. 4, in proc. of EPS-HEP Conference, Jerusalem, Aug. 19-26, 1997.
- [36] P.G. Jones, for the NA49 Collaboration, *Nucl. Phys. A* **610**, 188c (1996).
- [37] H. Appelshäuser *et al.*, NA49, *Phys. Rev. Lett.* **82**, 2471 (1999).
- [38] D. Evans, for the WA85-collaboration, *APH N.S., Heavy Ion Physics* **4**, 79 (1996).
- [39] D. Ferenc, U. Heinz, B. Tomasik, U.A. Wiedemann, and J.G. Cramer, *Phys. Lett. B* **457**, 347 (1999).
- [40] J. Cleymans and K. Redlich, *Phys. Rev. Lett.* **81**, 5284 (1998); and references therein.
- [41] J. Rafelski, pp 282–324, in *Future Relativistic Heavy Ion Experiments*, R. Bock and R. Stock, Eds., GSI Report 1981-6; in *New Flavor and Hadron Spectroscopy*, J. Tran Thanh Van, Ed. p 619, Editions Frontiers (Paris 1981); and in *Nucl. Physics A* **374**, 489c (1982).
- [42] F. Antinori *et al.*, WA85, *Phys. Lett. B* **447**, 178 (1999).
- [43] Th. Alber *et al.*, NA35, *Z. Phys. C* **64**, 195 (1994).
- [44] T.S. Biró, E. van Doorn, B. Müller, M.H. Thoma and X.-N. Wang, *Phys. Rev. C* **48**, 1275 (1993).
- [45] S.M.H. Wong, *Phys. Rev. C* **54**, 2588 (1996); and **56**, 1075 (1996), and references therein.
- [46] D.K. Srivastava, M.G. Mustafa and B. Müller, *Phys. Lett. B* **396**, 45 (1997); *Phys. Rev. C* **56**, 1054 (1997).
- [47] J.D. Bjorken, *Phys. Rev. D* **27**, 140 (1983).
- [48] J. Rafelski, J. Letessier and A. Tounsi, *APH N.S., Heavy Ion Physics*, **4**, 181 (1996);  
J. Letessier, J. Rafelski, and A. Tounsi, *Phys. Lett. B* **389**, 586 (1996).
- [49] <http://www.qm99.to.infn.it/program/qmprogram.html>  
Presentation on Friday, May 24, 1999 at 11:25AM by J. Rafelski; to appear in proceedings of *Quark Matter 1999*, Torino, Italy within a group report “*Last call for RHIC predictions*”. S. Bass *et. al.*, nucl-th/9907090.